Appendix F Constitutive equations for two-phase flow

Table of content

F.1 Introduction

Rock salt is considered to be a potential host rock for a deep geological repository for radioactive waste. With a view to robustness of the referring concept crushed salt from excavation is envisaged as a prime candidate for backfill material as it would show the highest compatibility with the host rock. Creep of the rock salt compacts the crushed salt leading eventually to an effective barrier against a possible brine inflow. If the crushed salt will have the favourable properties of undisturbed rock salt in terms of permeability and porosity is presently not entirely clear, though.

Because of the extremely low permeability of undisturbed rock salt it is expected that fluids will only enter the repository via shafts and drift seals. Eventually, the solution will also come into contact with the backfill. This implies that an initially dry section of the backfill will be wetted. Two distinct phases, air and brine, can subsequently be found in the pore space. The dynamics of the related wetting depend not only on porosity and permeability but also strongly on two constitutive relations (CRs): the capillary pressure-saturation relation (CPS) and the relative permeability-saturation relation (RPS) (e.g. /HEL 97/).

In a rigid matrix, as usually assumed for common soils, these properties suffice to describe groundwater flow mathematically. Crushed salt, however, is compacted by the creeping rock salt. The degree of compaction, quantified either by means of porosity or permeability, thus changes with time. The pore space decreases and concurrently the pore space topography changes. Note that the complexity of the wetting process is highly increased by the fact that backfill resistance to compaction decreases considerably with the wetting of the crushed salt. For a realistic prediction of the inflow dynamics into the backfill of a drift, a hydro-mechanically coupled model is thus essential.

The porosity-permeability relation that is required to describe single-phase flow in such an environment has been subject to numerous experimental investigations, and is rather well known (e.g. /KRÖ 09/). Despite the obvious necessity to consider unsaturated or two-phase flow in a repository, data on the CRs for crushed salt are still quite scarce. They are restricted to a certain degree of compaction, and are either providing only CPS /MAL 15/ or referring to a material of single grain size /CIN 06/. The data presently available therefore lacks information on relative permeability of crushed salt with a repository-

relevant grain size distribution as well as on the dependency of the CRs on the degree of compaction i.e. porosity.

The idea of applying Leverett's J-function to extrapolate the CPS must be dismissed as this scaling rule is based on the assumption of similarity of the pore space topography /LEV 41/. Furthermore this rule is known to fail for sand- and limestone if applied to permeability variations of more than two orders of magnitude /HAR 01/.

Presented here are therefore test results to derive CRs for crushed salt with a repository-relevant grain size distribution. The material is tested at different degrees of compaction and thus allows already for a first insight into the nature of CRs for repository-relevant backfill material as well as into the impact of compaction on the CRs.

F.2 Scope

During early stages of the post-operational phase the degree of compaction it is more comprehensibly characterized by its porosity as the crushed salt offers no significant resistance to flow. In advanced stages, by contrast, a comparatively little porosity decrease leads to permeability changes over orders of magnitude. For the investigations presented here, different degrees of compactions were chosen based on the following target brine permeabilities: 10^{-14} m², 10^{-15} m², and 10^{-16} m². Testing covered two pre-tests with samples called "P1" and "P2a" and "P2b", respectively, to demonstrate the feasibility of the test in general and to examine the test procedure. Due to a technical error during preparation, the unsaturated part of the actual first main test was spoiled. The single-phase flow parameters of the two referring samples "M0a" and "M0b", however, were determined. This was followed by the two main tests 1 and 2 with samples "M1a" and "M1b" as well as samples "M2a" and "M2b".

F.3 Preparations

Samples

Crushed salt from the Gorleben mine was used for the experiment. The grain density of the crushed salt material was measured to amount to 2,183 g/cm³. The grain size distribution was chosen to fit in with the possible backfill material that had been investigated

in several earlier projects on crushed salt (e.g. /ROT 99/, /KRÖ 15/, see Appendix G of the main report). Maximum grain size of the material was 8 mm.

Also determined was the initial moisture content, separately for each grain size fraction. The results are compiled in Tab. F.1.

Tab. F.1 Moisture content of Gorleben salt at delivery

Grain fraction [mm]	Mass fraction [%]	Moisture content [%]	partial moisture content [%]
4-8	10,56	0,03	0,0032
2-4	32,3	0,02	0,0065
1-2	23,23	0,03	0,0070
0,5-1	13,69	0,03	0,0041
0,4-0,5	4,46	0,04	0,0018
0,25-0,4	3,77	0,04	0,0015
0,125-0,25	6,32	0,04	0,0025
0,063-0,125	4,01	0,08	0,0032
<0,063	1,65	0,07	0,0012
sum	99,99		0,0309

Parallel measurements on crushed salt from the Gorleben site are reported in /ENG 12/. Ten samples each were taken from two different locations of recently excavated material showing a moisture content of 0.001 to 0.017 % and 0,008 to 0,027 %, respectively. The value of 0.031 % found here is slightly exceeding the values from /ENG12/. It has to be taken into account, though, that no particular care had been taken to ensure that freshly excavated material was obtained.

Note

– that the weighted mean of the moisture content is much lower than the value of 0.1 % determined for the material from the Asse mine,
– that the moisture content appears to be invers proportionally related to the grain size which is probably a result of the size-dependent surface to volume ratio, and
– that a simple arithmetic mean amounting to 0.0422 would have been quite misleading.

Samples were prepared in a hollow steel cylinder by axial compaction from both sides. Tentatively prepared samples under compaction from just one cylinder end had shown in ultra-sonic control measurements a considerable inhomogeneity along the sample axis. The resulting density distributions for both compaction methods are depicted in Fig. F.1. Note that the porosity values given in Fig. F.1 are quite roughly estimated and can thus only be interpreted in relation to other values in this graph. Note furthermore that greasing the inner cylindrical wall to minimise friction during the compaction had no noticeable effect.

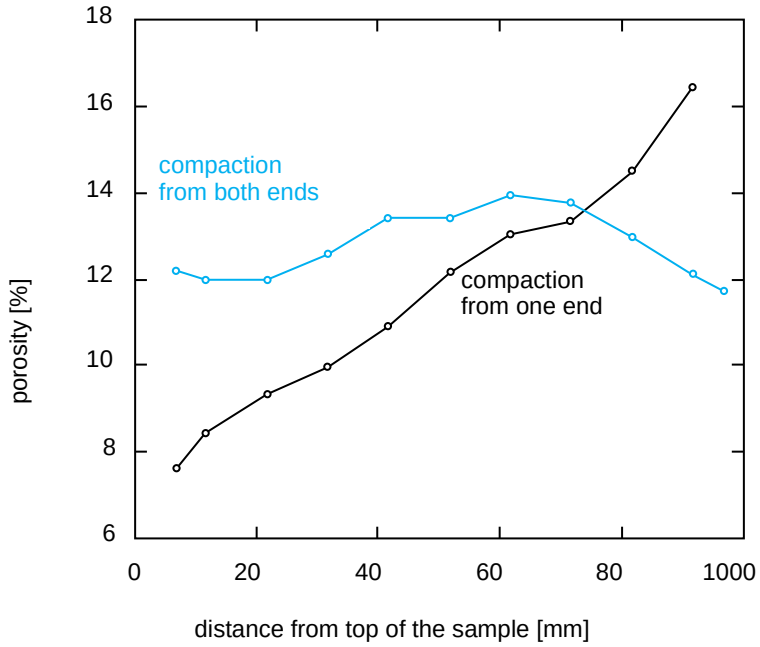

Fig. F.1 Axial density distributions resulting from different compaction methods.

The cylindrical samples had a designed length of 100 mm and a diameter of 50 mm. The amount of crushed salt material required for the samples thus depended on the respective target porosity, 10 %, 7.5 %, and 5.5 % which was derived from a data compilation for the porosity-permeability relation of crushed salt /KRÖ 09/ to meet the previously defined target brine permeability values.

Fluids

The brine used in the test had to be saturated with the same salt with which the samples had been prepared to avoid solution of sample material in the presence of brine. Determined in the laboratory were a density of 1.20157 g/cm³ and a viscosity of 2.303 mPa*s.

Nitrogen was used where gas was involved in the test. Since all measurements were performed under room temperature the related gas viscosity was 0.0174 mPa*s.

F.4 Test procedure

For each test several cylindrical samples were prepared to match a target permeability which was checked by gas permeability tests of the air-dry samples (see Appendix). Well-suited samples were flooded with the pressurized saturated salt solution applying additionally a vacuum at the other end of the sample to minimize the remaining air saturation. Subsequently, the brine permeability was measured. The single-phase flow parameters for all samples are compiled in Tab. F.2 (see section F.9).

Unsaturated conditions were initiated by applying gas pressure at one side of the sample while monitoring the opposite side for gas and brine outflow. The gas pressure was carefully increased in steps to identify the gas entry pressure as it can only be narrowed down to the range between two consecutive gas pressure levels.

When outflow occurred and came close to steady-state the amount of expelled brine allowed calculating the actual brine saturation of the sample. This saturation together with the related injection pressure constituted the first point in the CPS-curve. The gas outflow rate, observed in parallel, lead to an effective gas permeability providing eventually the first point of the RPS-relation.

Further points constituting these curves were gained by the same procedure: increase the gas pressure, measure brine outflow until reaching equilibrium and measure the related gas permeability.

The test was terminated when the increase of injection pressure did not result in further brine outflow. After dismantling the sample the remaining amount of brine was measured for a consistency check of initial brine content and outflow against the final brine content.

Note: The test set-up is not entirely consistent with an inflow scenario. It is rather applicable to a situation where the backfill is already fully brine saturated and gas production starts to de-saturate the backfill again.

F.5 Pre-test 1

The pre-test was performed in a Hassler-type cell (see Fig. F.2). To prevent the testing fluids from circumventing the sample during hydraulic testing the sample was placed in a rubber jacket which was then loaded by a circumferential pressure exceeding the injection pressure by 2 bar.

Sample P for the pre-test had a porosity of 7.33 % which was slightly below the target value. Three different measurements of the gas permeability amounted nevertheless to a mean value of 7.5·10-15 m² which was somewhat higher than expected. Also not expected from previous experience was the fact that the brine permeability amounted to about the same value as the gas permeability.

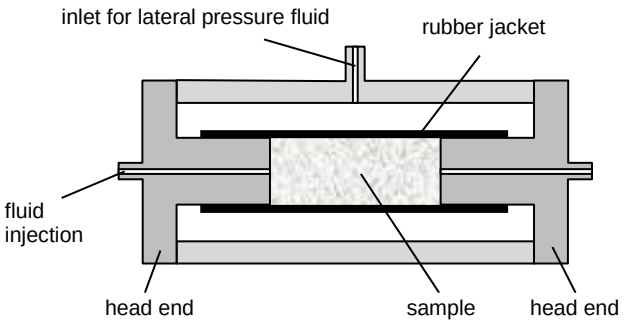

Fig. F.2 Sketch of the test cell for the pre-test.

The results of the pre-test have been published /KRÖ 15/ and are summarized in Fig. F.3 and Fig. F.4. Note that the empty symbols represent uncharacteristic measurement conditions and should thus be disregarded. Air entry pressure in the CPS lay between 50 and 100 mbar. The maximum injection pressure amounted to about 15 bar in this test. Residual brine saturation lay at 38 %.

While both curves show a characteristic shape, relative permeability at residual brine saturation was conspicuously low. To find an explanation for this observation, a final brine permeability test[1] was initiated. It was performed over several days at different pressure gradients and resulted in a characteristic value of $4.9 \cdot 10^{-16}$ m². This is more than

[1] Drying the sample in the oven to clear the pores for another gas permeability test was out of question because it would have changed the topology of the pore space by crystallisation.

one order of magnitude lower than the value of $7.5 \cdot 10^{-15}$ m² measured at the beginning of the test.

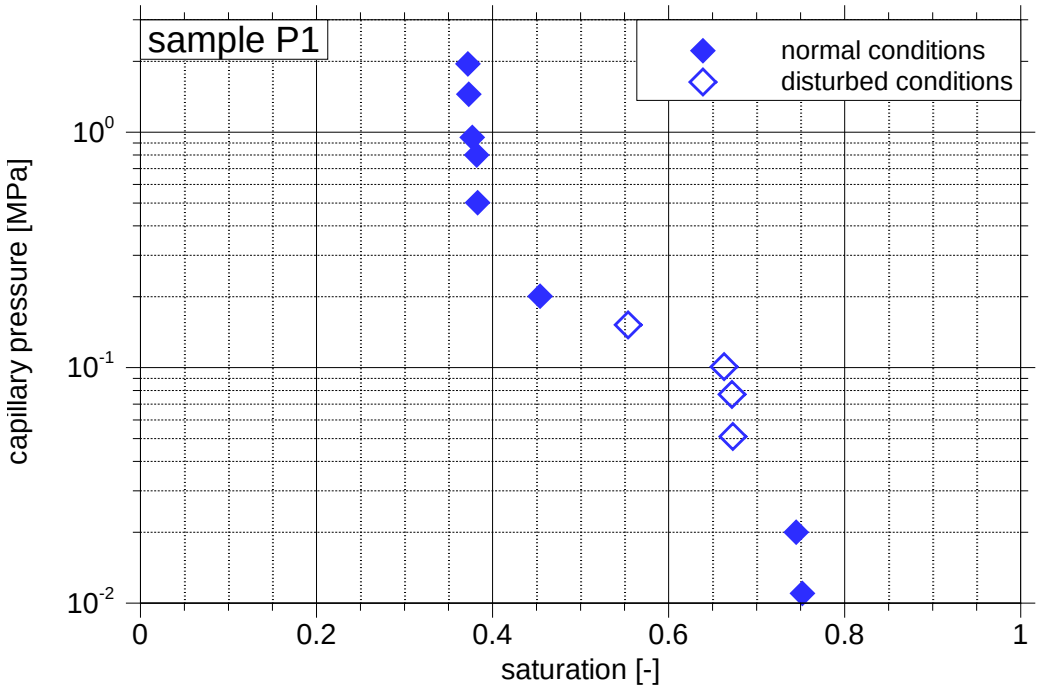

Fig. F.3 CPS for sample P1; from /KRÖ 15/.

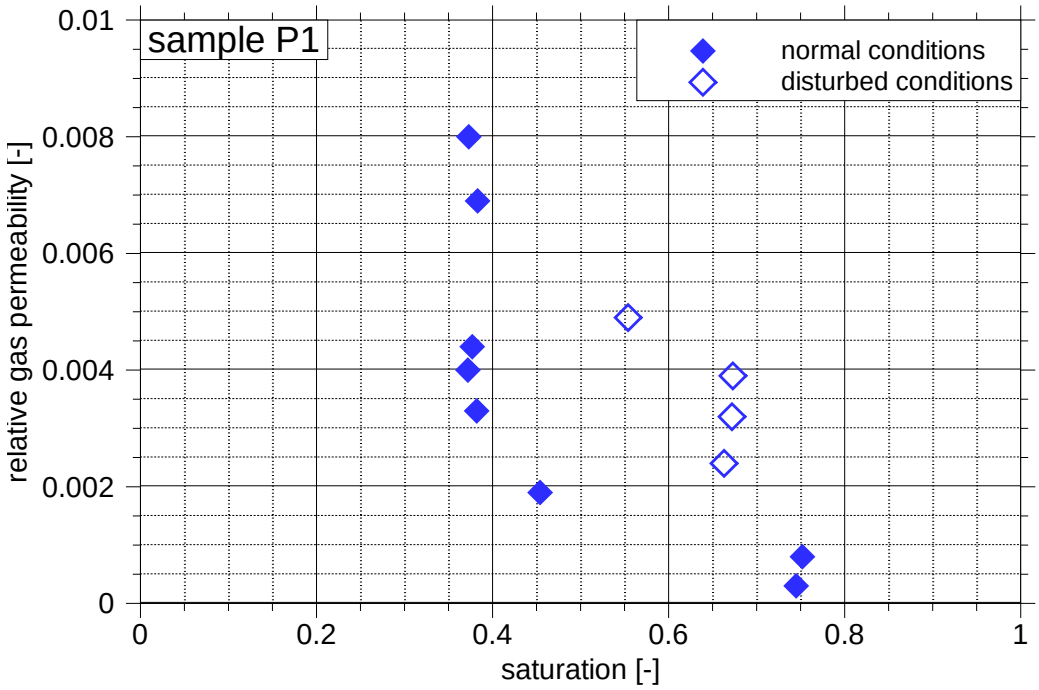

Fig. F.4 RPS for sample P1; from /KRÖ 15/.

It was thus suspected that the brine in the pore space had reduced the mechanical resistance to compaction to the point where the overpressure on the rubber jacket would result in a significant reduction of the pore volume and thus of the single-phase gas permeability. To check this effect a second pre-test was performed.

F.6 Pre-test 2

To investigate the effect of a possible compaction due to the hydraulic pressure that was applied to the rubber jacket, two more samples – P2a and P2b – were prepared for permeability tests. The samples had a porosity and a gas permeability of 8.13 % / $1.7 \cdot 10^{-14}$ m² and 7.43 % / $1.3 \cdot 10^{-14}$ m², respectively.

After measuring the gas permeability the samples were saturated under vacuum and installed in the Hassler cell. Saturated brine was then injected as in pre-test 1. After breakthrough it was additionally circulated to minimise possible solution or precipitation effects in the pore space. Fig. F.5 shows the evolution of the brine permeability for samples P2a and P2b.

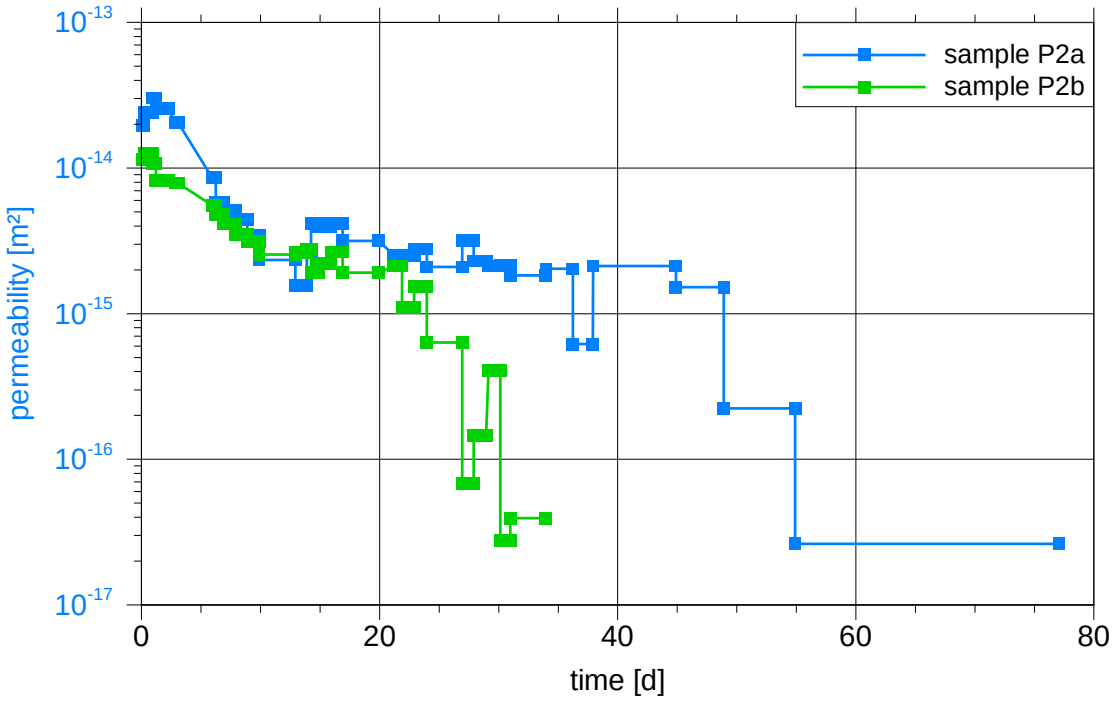

Fig. F.5 Brine permeability in tests with samples P2a and P2b

The data shows a more or less linear decline of the permeability for both samples from $2.0 \cdot 10^{-14}$ m² to $2.0 \cdot 10^{-15}$ m² and from $1.1 \cdot 10^{-14}$ m² to $2.0 \cdot 10^{-15}$ m², respectively, over a period of about 10 days. After these 10 days, the permeability value does not change significantly for some time (38 and 14 days, respectively) before the permeability decreases quickly. The curves end when no outflow could be measured within the accuracy of the test method.

The first decline of permeability was interpreted as the result of the overpressure from the rubber jacket while no conclusive explanation could be found for the second and final decrease. To avoid this effect the test design was changed for the main tests. As it turned out later, though, this did not help to prevent a considerable decrease of the permeability.

F.7 First main test

Due to a technical error during preparation, the unsaturated part of the test was spoiled. The single-phase flow parameters of the two referring samples, however, were determined and are included in Tab. F.2 labelled “main test 0”.

F.8 Main test 1

Set-up and results

While sample preparation was performed for the main test as in the pre-test, the samples for the main tests were afterwards inserted in steel tubes instead of a Hassler cell to avoid the suspected compaction from the excess pressure on the rubber jacket. The remaining annulus between sample and tube was filled with a low-viscosity epoxy resin. To ensure that only the annulus was filled but not the pores of the sample, a tentatively prepared sample was opened up with a saw. Very little of the epoxy resin, indeed, had entered the pore space thus leaving the sample basically free of alterations as shown in Fig. F.6. The whole improved test set-up is sketched in Fig. F.7.

Fig. F.6 Intrusion of coloured resin into the pore space of a compacted sample

The test procedure was essentially the same as in the pre-test. However, more emphasis had unintentionally been placed on reaching steady-state in the outflow and to ensure full collection of brine during each pressure level as close as possible. The resulting evolution of injection pressure, cumulative mass of brine and gas permeability is shown in Fig. F.8 and Fig. F.9.

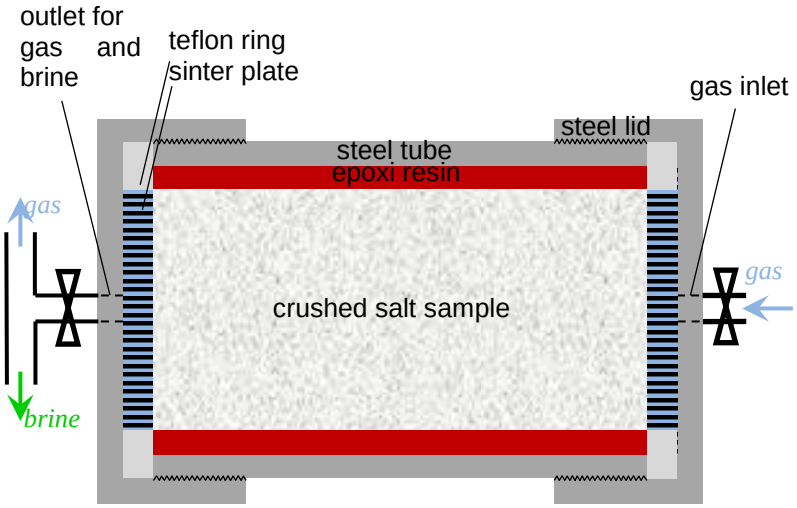

Fig. F.7 Improved test set-up (sketch true to scale).

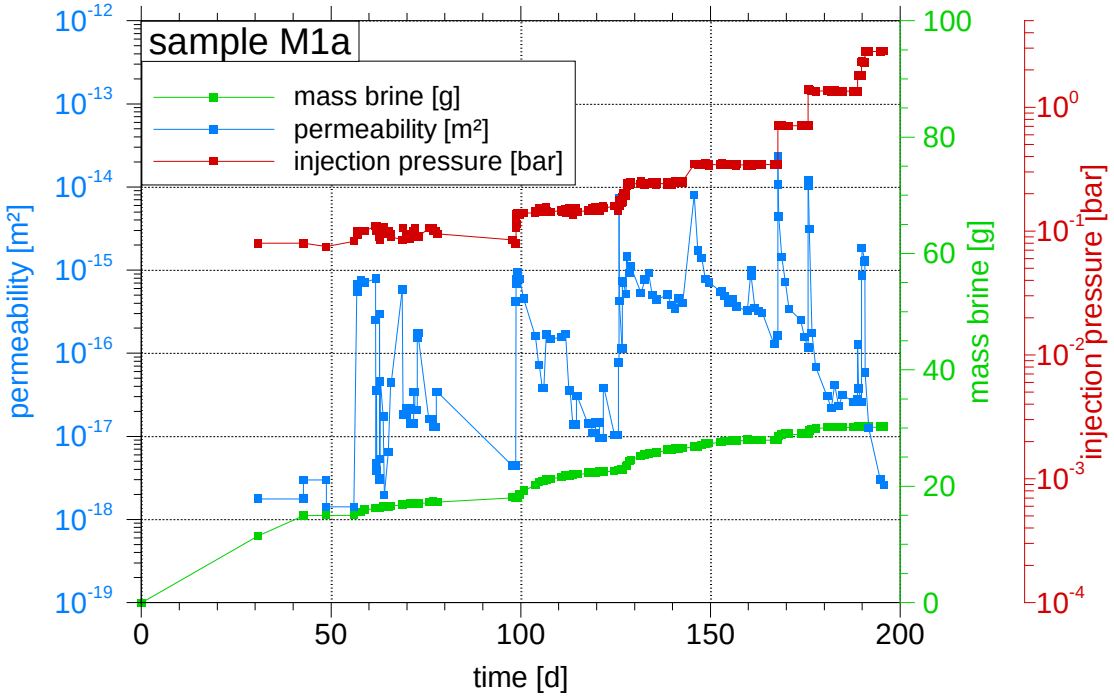

Fig. F.8 Measured data for sample M1a.

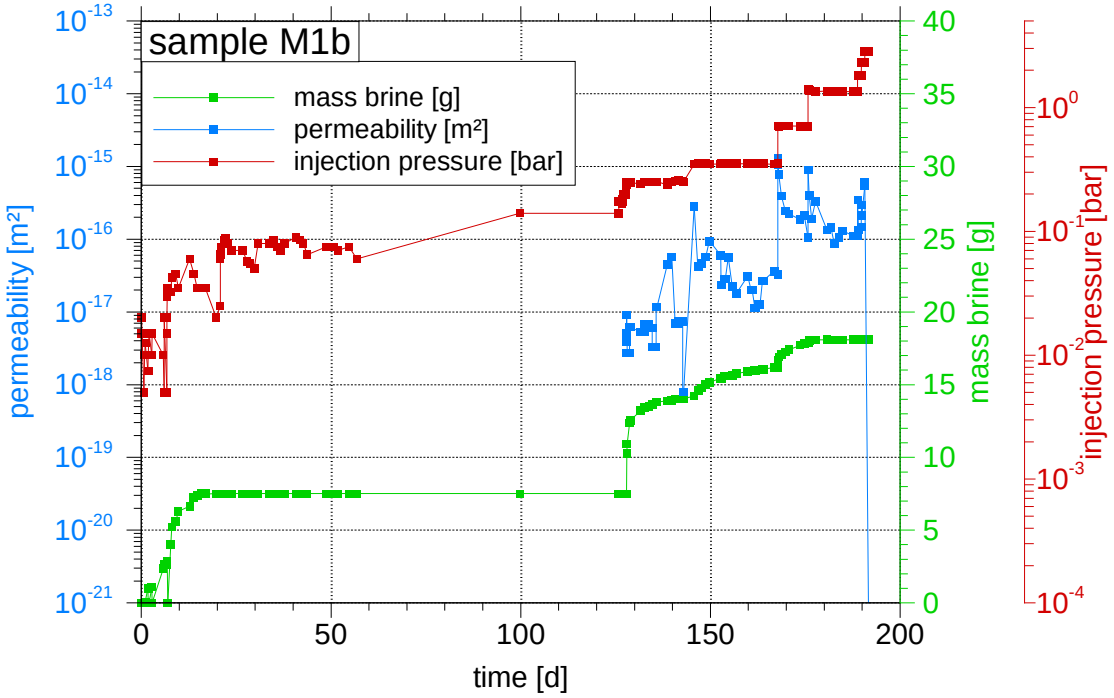

Fig. F.9 Measured data for sample M1b.

Brine flow from sample M1a began at an injection pressure of 30 mbar and first gas flow was observed at about 75 mbar injection pressure. Sample M1b showed outflow more or

less right at the beginning of the test but no accompanying gas flux. Outflow stopped then and recommenced only at about 250 mbar. At this pressure level gas flow set in as well.

Evolution of gas outflow and the related effective gas permeability in the test is rather complex. It can be summarized by five observations:

– Each increase of the injection pressure (after the onset of gas flow) was accompanied by a sharp and high increase of gas flow that was followed by a seemingly exponential decrease of the flow further on.
– The effect of decreasing gas permeability became better visible with increasing injection pressure as the noise in the data decreased.
– The decrease of gas permeability took increasingly less time with increasing injection pressure.
– The dynamic range of the decrease was significantly larger in sample M1a than in the less permeable sample M1b.
– Towards the end of test, particularly in sample M1a, also the peak values decreased with increasing injection pressure.

After terminating the test, the samples were carefully dismantled. The amount of brine remaining in the sample at end-of-test was determined by drying at 105 °C over 24 hours, taking into account that heating would expel the water but not the dissolved salt. Furthermore, the amount of brine remaining in the test apparatus outside the sample was determined as well. These data were used to check the consistency of the amount of brine that had been taken up during sample saturation before the test and the sum of expelled brine, brine in the apparatus and brine in the sample at end-of-test.

At end-of-test 6.05 g of brine (sample M1a) and 3.47 g (sample M1b), respectively, appeared to be missing. This loss is attributed to evaporation of water from the pore space as it was despite great effort not possible to saturate the nitrogen completely up to the relative humidity of 76 % which is related to the partial vapour pressure over a saturated salt solution. The resulting reduction of the pore space amounted to 8.6 % and 7.1 %, respectively. The resulting residual brine saturation in the samples amounted to 11.6 % and 35.3 %, respectively.

Interpretation

Explanations for the five observations listed in the previous section require a deep insight into the processes involved in the test. Outflow of solution from sample M1b at the initially very low injection pressure is interpreted as brine flow through the sample draining the design-inherent unavoidable additional brine-filled volume at both ends of the cell. Air entry pressure was reached only when gas was flowing through the whole sample. This happened at 75 mbar injection pressure in case of sample M1a and at 250 mbar in case of sample M1b. Air entry pressure could thus be narrowed down to the ranges between 40 and 75 mbar for sample M1a and 140 and 250 mbar for sample M1b.

The decrease of gas permeability during each load step is interpreted to be a consequence of a complex interplay of several effects and processes. The first consideration here is that the local gas pressure in a sample is conveyed via the capillary pressure also to the liquid phase thereby introducing a pressure gradient in the liquid phase as well. As a consequence, a certain brine displacement towards the outlet is suspected to occur. In the presence of open flow channels for the gas, however, this does not necessarily result in an outflow of brine from the sample. A fraction of the brine mass might as well simply have been redistributed along the sample axis, more precisely from the inlet towards the outlet because in this case the local brine saturation increases with a decreasing gas pressure. As a result the flow channels for the gas become widened at the inlet and at the same time constricted at the outlet forming a bottleneck for gas flow at the outlet.

Generally, brine displacement by gas in the pore space of the sample comes to an end when the gas pressure reaches equilibrium with the antagonizing capillary pressure. Due to the complexity of this process the conditions at steady-state are hard to predict. It is thus that two characteristic properties of the gas permeability evolution – the strong decrease after increase of the injection rate and the rapidness of this process increasing with the injection pressure – could only be explained in hindsight. Qualitatively, the effect itself appears to be a consequence of redistribution while the process velocity is controlled by the pressure gradient in the liquid phase.

Against this background the acquired data were processed according to the following heuristic rules:

– Daily averages of the up to four measurements per day were calculated from the roundabout 550 data points forming the basis of the subsequent evaluation.
– Capillary pressure was assumed to be the injection pressure.
– The effective gas permeability at a specific degree of saturation was assumed to be the mean of all values within a range of no more than one order of magnitude below the peak value.
– To compensate the error from the brine in the free space of the test apparatus on the calculated brine saturation of the sample, an artificial linear correction of the expelled brine mass with time was introduced in such a way that the measured end-of-test brine saturation was met.

The resulting data are visualised in Fig. F.10. Besides the trustworthy data, marked with full symbols and lines, two other categories of data are distinguished here: (a) data with some sort of uncertainty because of a continuous decrease of gas permeability during the overly long equilibration period are called “unreliable” and are marked with open symbols and lines; (b) data that were obviously spoiled by the too long equilibration periods showing lower instead of higher gas permeability are marked with open symbols only. The data confirm the observation from the previous section – particularly on sample M1a – about the unexpected decrease of relative permeability towards the end of the test. The effect is also reflected in the capillary pressure data where the upwards trend with decreasing brine saturation is seemingly interrupted as no further outflow of brine was measured.

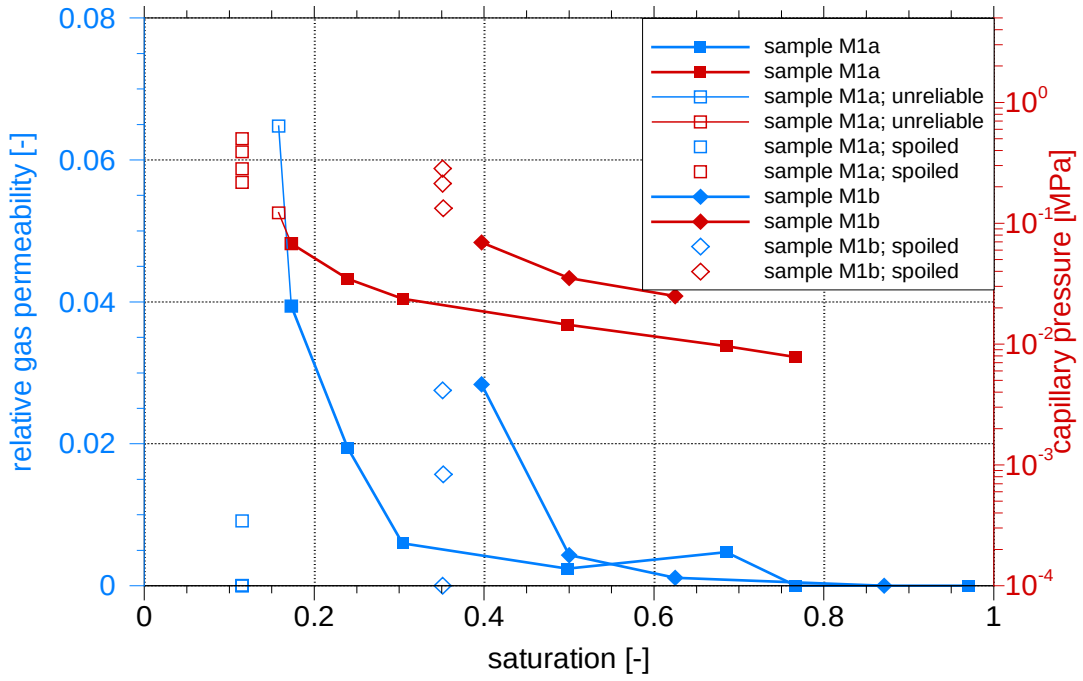

Fig. F.10 RPS and CPS for samples M1a and M1b.

Conclusion for main test 1

With a view to the test procedure two antagonistic demands concerning the duration of each load step were found. On the one hand the test should run until brine outflow comes to an end in order to get a good approximation of the saturation. But on the other hand it should proceed quickly to the next load step to avoid advective re-distribution of pore water due to differences in capillary pressure. In the end it appears that the decision about a good compromise between these two demands and when to end a test step remains in the judgement of the experimentalist. At least two possible sources of errors in the data from main test 1 could thus be identified: redistribution of brine along the sample axis caused by the gas pressure gradient and crystallisation due to undersaturated nitrogen gas.

All reliable data for the RPS lie in the same region below a relative permeability of 0.01 as in the pre-test. It appears that the relative gas permeability increases only when the saturation is approaching the residual brine saturation. The curiously low data values observed in the pre-test thus seem not to have been caused by excess pressure at the rubber jacket but rather by a pore space changing process such as salt redistribution by pressure solution. This has to be looked into in detail yet.

F.9 Main test 2

As a consequence from the first test for conducting main test 2 the following measures were adopted:

– A load step was intended to be terminated before brine outflow stopped completely. Each ad hoc decision to do so had to be based on the data collected so far.
– A mean of the first few gas permeability values in a new load step was adopted as the basis for the related relative permeability.
– A cascade of two wash bottles instead of just one for wetting the nitrogen was used.

Generally, during main test 2 some limits in the applicability of the chosen measuring method became apparent. The first such indication came up during the measurement of the brine permeability of sample M2a. Permeability was more or less stable slightly above 10^{-15} m² until the injection pressure was increased to 3 bar. All of the sudden, outflow increased to the extent that the injection pressure broke down and the apparent permeability increased by three orders of magnitude as shown in Fig. F.11. This event compromised sample M2a and no meaningful data for unsaturated conditions could be collected further on.

Later, at the end of the experiment, the samples had to be removed from the test cells. This was begun by repeatedly dropping cell and sample into a pot of boiling water in order to dissolve the salt. After the first such dissolution of salt the outer sections of compacted salt had vanished. Inspection showed that sample M2a had indeed been structurally compromised. A big hole could be observed at both ends of the tests cell which appear to have been connected by a considerable hole (see Fig. F.12) underpinning the notion of a forced channel through the sample.

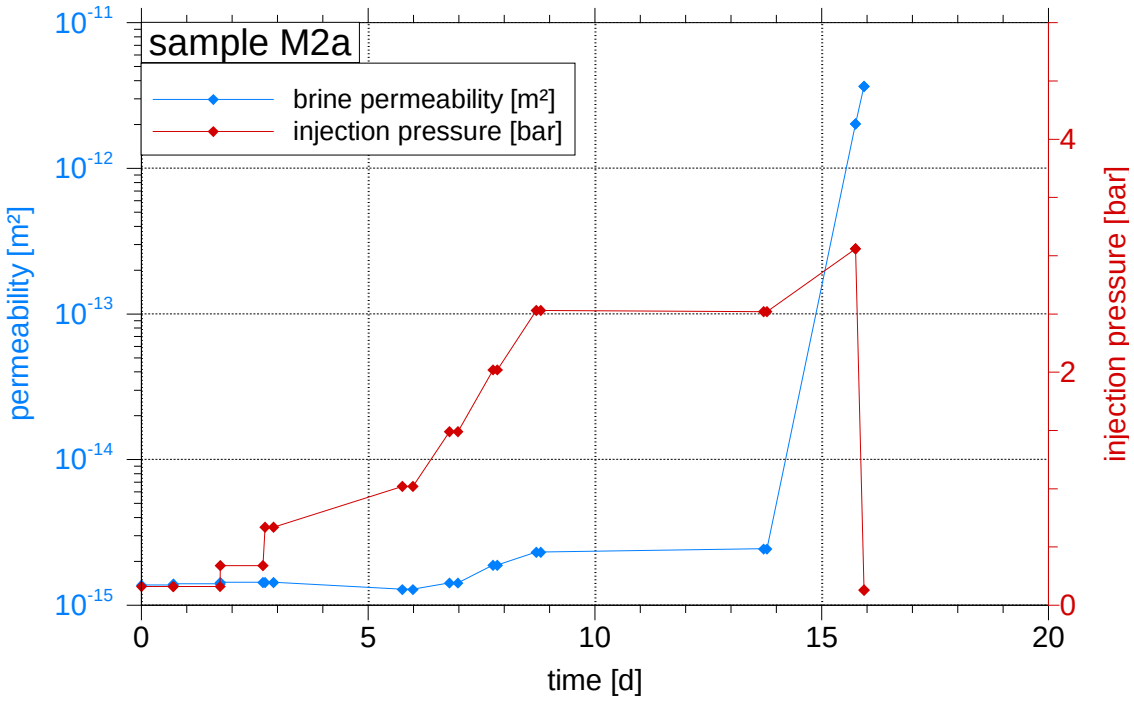

Fig. F.11 Brine permeability measurement data for sample M2a.

Fig. F.12 Top and bottom of sample M2a after some dissolution in boiling water.

By contrast, sample M2b showed no such behaviour in the course of testing, even at 4.5 bar. The amount of expelled brine, however, was quite small (see Fig. F.13), meaning that a more advanced compaction would probably have resulted in even less outflow rendering recognition of changes in the brine saturation virtually impossible.

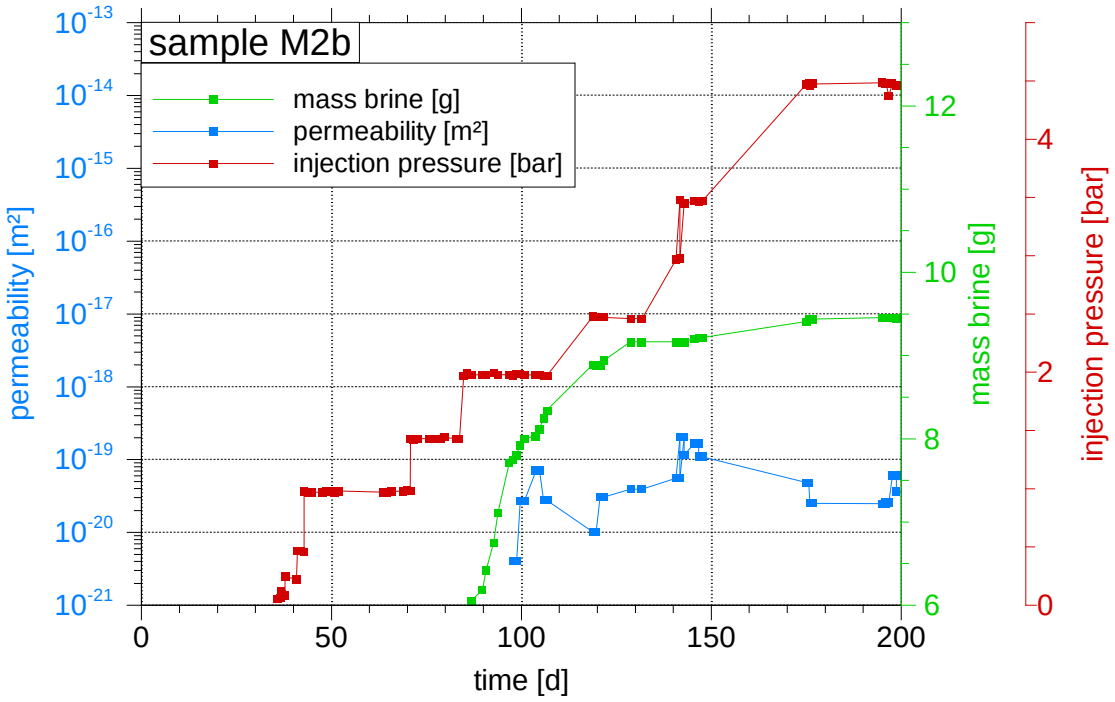

Fig. F.13 Measured data for sample M1b.

F.10 Check of single-phase permeabilities

The relevant single-phase flow parameters for all samples are compiled in Tab. F.2. To check the consistency with earlier data, the single-phase permeabilities are compared to a compilation of data on the porosity-permeability relation of crushed salt /KRÖ 09/ as depicted in Fig. F.14. Also included in the graph are the data from the new test D-A-025 presented in section 2.5.1 of the main report. Note that tests with spindle oil provided the same results as the tests with nitrogen. The permeability values determined in this project are denoted by coloured symbols. They fit well into the ranges of uncertainty that come with the earlier data.

In case of pre-test 2 with brine the range between the first measured permeability value as well as the temporary constant value (cp. section F.6) are indicated in Fig. F.14. It appears that the lower permeability value generally fits much better into the previously derived range of values than the initial one.

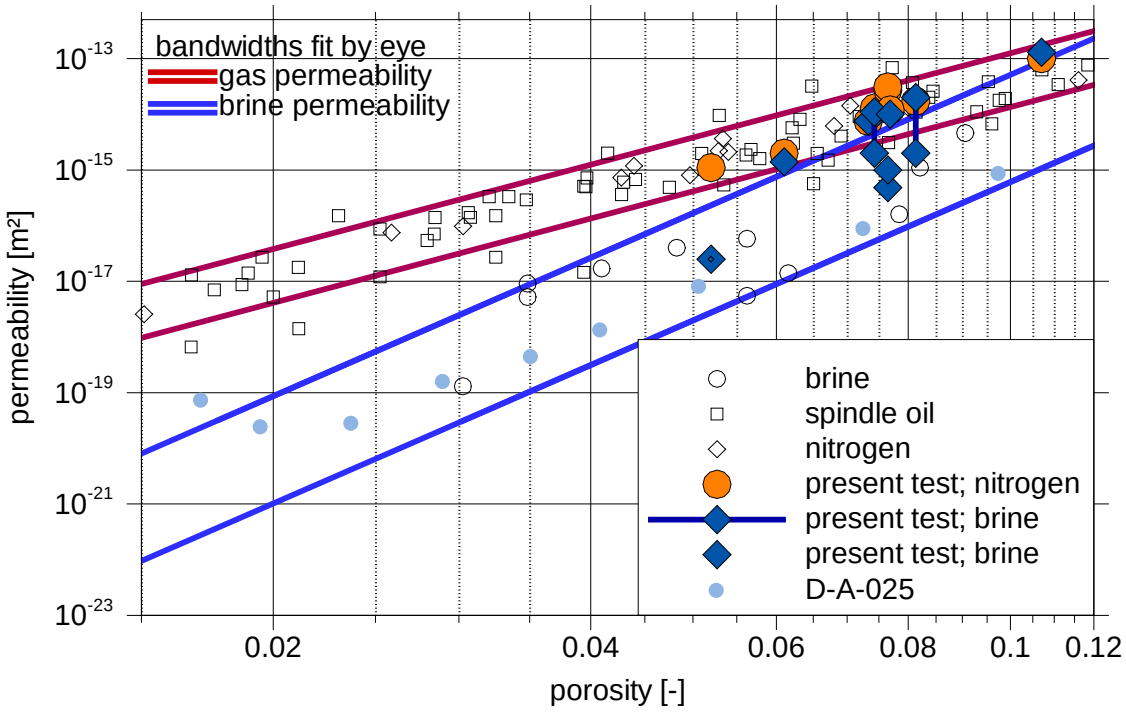

Fig. F.14 Consistency of measured permeabilities; modified from /KRÖ 09/.

Tab. F.2 Compilation of single-phase flow parameters

Sample	Porosity [%]	Gas permeability [m²]	Brine permeability [m²]
P1	7.33	$7.5 \cdot 10^{-15}$	$7.5 \cdot 10^{-15}$
P2a	8.13	$1.7 \cdot 10^{-14}$	$2.0 \cdot 10^{-15}$ - $2.0 \cdot 10^{-14}$
P2b	7.43	$1.3 \cdot 10^{-14}$	$2.0 \cdot 10^{-15}$ - $1.1 \cdot 10^{-14}$
M1a	10.70	$1.0 \cdot 10^{-13}$	$1.3 \cdot 10^{-13}$
M1b	7.69	$1.2 \cdot 10^{-14}$	$1.0 \cdot 10^{-14}$
M2a	6.10	$2.0 \cdot 10^{-15}$	$1.4 \cdot 10^{-15}$
M2b	5.20	$1.1 \cdot 10^{-15}$	$2.5 \cdot 10^{-17}$

F.11 Compilation of CRs for all tests

Directly measured data

Supplementary sample data for two-phase flow concern the bounding values for the air entry pressure and the residual brine saturation. They are compiled in Tab. F.3.

Tab. F.3 Supplementary two-phase flow data

Parameter\ Sample	P1	M1a	M1b	M2b
$p_{e,}$ lower bound [MPa]	0.0050	0.0040	0.0140	0.14
$p_{e,}$ upper bound [MPa]	0.0100	0.0075	0.0250	0.20
S_{rb} [-]	0.38	0.115	0.35	0.43
S_{rg} [-]	0.25	0.03	0.13	0.44

CRs from data

The compiled data on the CRs that have been derived from the tests are presented in Fig. F.15. The CPS curves seem to follow the classical two-phase flow theory. This applies also to sample P1 despite the different set-ups for the pre-test and for the main tests. As expected, the capillary pressure increases inverse proportionally to the porosity.

It had also been expected that the residual brine saturation as well as the air entry pressure increase with decreasing porosity. This has been confirmed by the measurements even if it has to be conceded that in case of the residual saturation the derived values for samples M1a and M1b might be erroneous due to the long equilibration periods during the first main test.

The RPS curves, however, deviate from the classical two-phase flow theory. Relative gas permeability is very low over a wide range of saturations and appears to increase strongly only in the vicinity of the residual brine saturation. The close-up of the RPS curves in Fig. F.16 illustrates that the data do not show conclusively whether a dependency on the porosity exists in the low value range at all. This observation remains the same if the results of the pre-test fit are included.

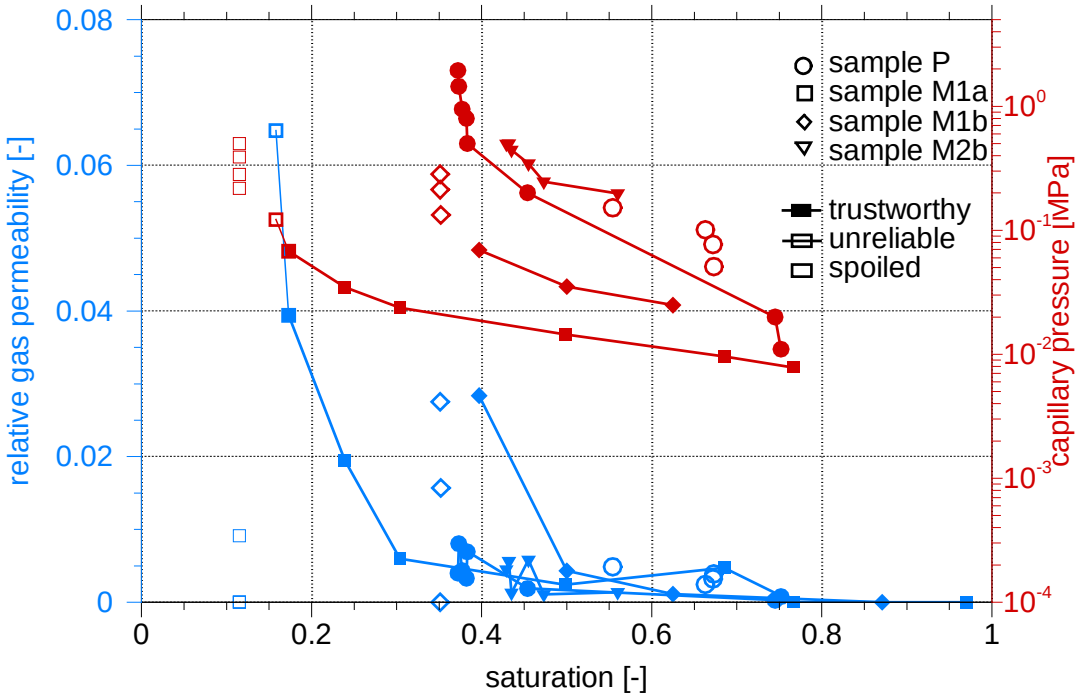

Fig. F.15 RPS and CPS for all samples.

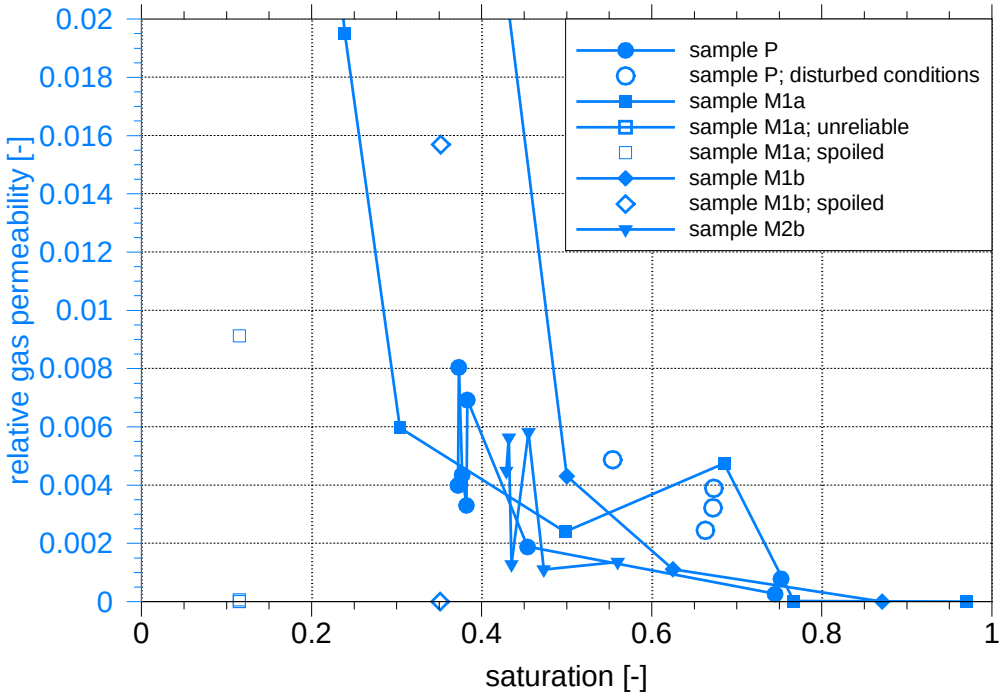

Fig. F.16 RPS for all samples; close-up.

Fitting a Brook-Corey approach to the data

A well-known approach for the CRs was formulated by Brooks and Corey /BRO 64/:

$$p_c = p_e \cdot S^{-\frac{1}{\lambda}} \qquad (F.1)$$

$$k_{rw} = S^{\frac{2+3\lambda}{\lambda}} \qquad (F.2)$$

$$k_{rnw} = (1-S)^2 \cdot (1-S^{\frac{2+\lambda}{\lambda}}) \qquad (F.3)$$

p_c - capillary pressure [Pa]
p_e - air entry pressure [Pa]
λ - coefficient of the pore size distribution [-]
k_{rw} - relative permeability of the wetting phase [-]
k_{rnw} - relative permeability of the non-wetting phase [-]

It is largely equivalent with the approach of van Genuchten /GEN 80/ as shown in /LEN 89/ but has the obvious advantage that it acknowledges the air entry pressure directly in the formulations. Each of the measured CPS curves can reasonably well be reproduced by a Brooks-Corey approach as shown in Fig. F.17. The resulting fitting parameters are compiled in Tab. F.4. Differences between the pre-test and the first main test can clearly be seen in Fig. F.17 as the shape of the curve for the pre-test does not fit in with the shape of the other three.

Tab. F.4 Compilation of parameters for the Brooks-Corey approach fitting the CPS

Parameter	Sample P1	Sample M1a	Sample M1b	Sample M2b
porosity	7.33 %	10.7 %	7.69 %	5.2 %
λ	0.6	1.2	1.7	3
air entry pressure	0.01 MPa	0.007 MPa	0.015 MPa	0.170 MPa
residual brine saturation	0.372	0.115	0.35	0.43
brine sat. at resid. gas sat.	0.75	0.97	0.87	0.56

Depicted in Fig. F.18 are the RPS curves that were also calculated with the parameters from Tab. F.4. A comparison of the calculated with the measured curves indicates no relation at all. This did not change when using even extreme λ-values.

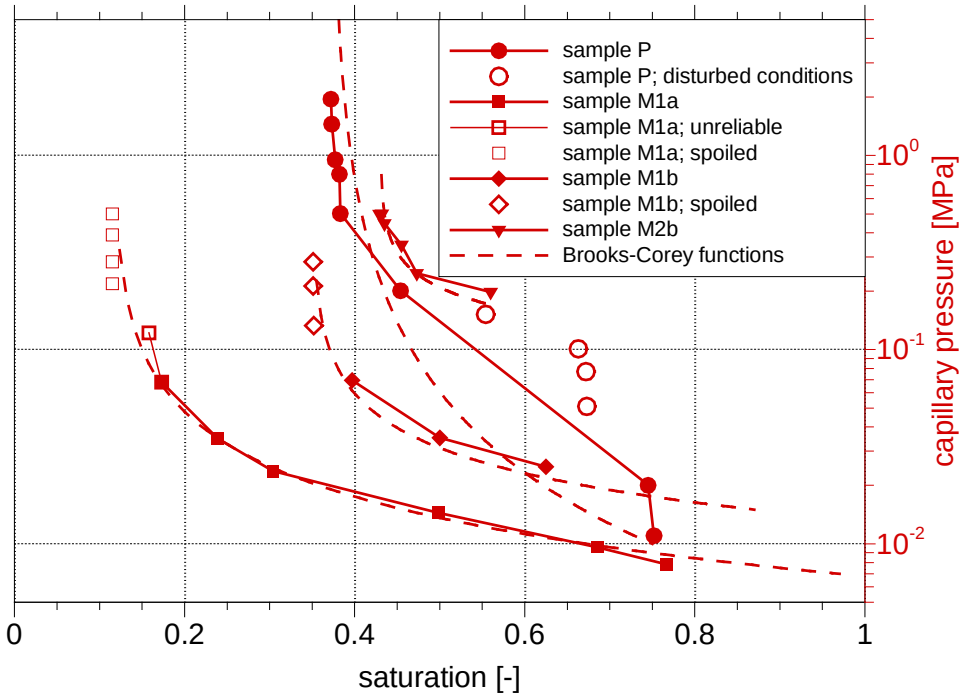

Fig. F.17 Measured and tentatively fitted CPS'.

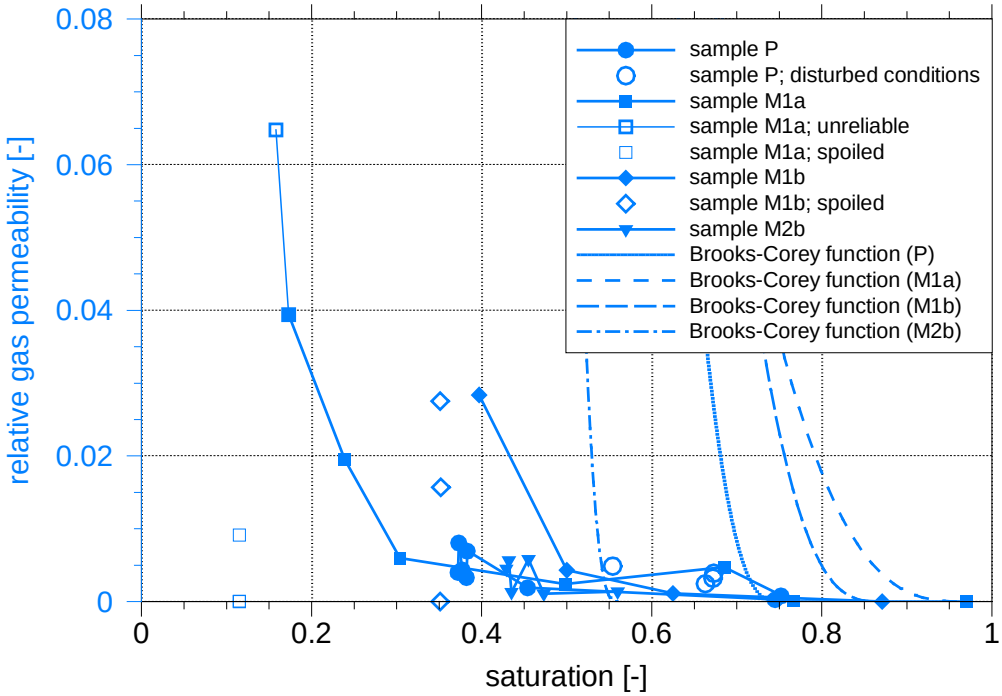

Fig. F.18 Measured and tentatively fitted RPS'.

F.12 Summary and discussion

Two pre-tests and two main tests were performed providing a total of 4 data sets to derive constitutive equations for the capillary pressure and the relative permeability of compacting crushed salt. The single-phase flow data for gas and brine permeability follow previously derived porosity-permeability relations within the observed uncertainties. Air entry pressure and residual brine saturation develop according to the expectation that both values increase with decreasing porosity.

Each of the measured CPS curves is also consistent with the two-phase flow theory for common soils and could thus be fitted reasonably well with the approach of Brooks and Corey. The curves show the expected general increase of capillary pressure with decreasing porosity. However, with only three comparable CPS curves available, it does not make sense, yet, to formulate a dependency on porosity.

The RPS curves for gas showed by contrast such a big difference to the classical two-phase flow theory that reproducing the individual RPS curves even with extreme parameter values failed. This is a considerable drawback because it means that the theory of Brooks and Corey fails for compacting crushed salt. It is apparently not possible to derive the RPS from parameters for the CPS as the work of Brooks and Corey implies. While new formulations for the RPS can certainly be found, the RPS for brine can thus not be predicted on a purely theoretical basis. Consequently, this calls for different tests that provide data for brine permeability under unsaturated conditions.

A second conclusion from the measured RPS curves concerns the relation to the degree of compaction. In principle, the RPS curves for gas look the same for all samples. They are remarkably gently inclined resulting in very low values except in the immediate vicinity of the residual brine saturation. Here, the relative permeability increases strongly. The only difference between the RPS curves thus seems to be the saturation range limiting residual brine saturation. Note that it is presently not clear if the single-phase gas permeability had remained unchanged and a relative permeability of “1” could have actually been reached in the experiment.

The results from the second main test indicate the limits of the test procedure when it comes to low permeabilities. An advanced degree of compaction beyond a brine perme-

ability of 10^{-17} m² or a porosity of less than 5 % could not have been tested with the procedure followed in this experiment.

Two-phase flow in general is a highly non-linear process /HEL 97/. Erroneous CRs can have a much bigger impact on the results than merely badly chosen single-phase parameters as they may change the flow dynamics not only quantitatively but also qualitatively. Minimisation of uncertainties in the CRs must therefore have high priority for reliable two-phase flow simulations. Considering the limited amount of tests, the present experiment can thus provide not more than a first impression of the CRs for compacting crushed salt. Concrete predictions based on these results are therefore not advisable. Against this background further testing is recommended to quantify the range of uncertainties.

Additionally, it has to be pointed out that the crushed salt material investigated here was well-defined and of a comparatively high degree of homogeneity. This did not prevent the failure of sample M2a during the measurement of brine permeability. A much higher range of data scatter is to be expected from the uncertainties caused by the backfill preparation under in-situ conditions in an operational repository. This effect has to be taken into account because otherwise, it will eventually compromise the validity of predictions concerning two-phase flow.

Further testing of the CRs for crushed salt should also focus conceptually on a realistic representation of the two-phase flow process in question. One concern should relate to the wetting dynamics in the test. In the experiment presented here the samples were stepwise desaturated beginning at full brine saturation. Inflow into a real repository, by contrast, would begin at a comparatively dry state of the backfill and lead to an increasing brine saturation. This process can later be reversed, though, if gas production kicks in and desaturates the backfill again.

An additional argument pointing in the same direction can be derived from the surprisingly low relative gas permeabilities in both of the experimental set-ups. The fact that they were observed independently of a circumferential pressure indicates another pore volume changing process like re-distribution of salt on the pore scale. The CRs and thereby the flow dynamics in general might thus be strongly influenced by the underlying wetting scenario and in particular by the initial conditions for which the test is conceived.

Another concern arises then from the idea of salt re-distribution. The phenomenon of pressure solution at the contact between two salt grains that are mechanically squeezed together is a well-established fact. Further hydraulic tests under compacting conditions might therefore be advisable.

It thus appears that the robustness of the safety case regarding the compaction of crushed salt must be strengthened. As long as it is relying on quantitative two-phase flow calculations for the backfill it is unavoidable to perform an extensive laboratory program with the following agenda:

– determine the RPS for brine directly,
– determine the uncertainties related to inhomogeneities in the grainy backfill material under laboratory and under operational conditions
– quantify the uncertainty in the dependency of the CRs on different degrees of compaction,
– determine the impact of a mechanical load on the CRs, and
– determine the impact of different wetting conditions on the CRs.

The decision about which alternative should be followed in the future should be carefully considered as it is foreseeable that modifying the safety case as well as investigating two-phase flow properties of crushed salt will require substantial effort.

References

/BRO 64/ Brooks, R.H., Corey, A.T.: Hydraulic Properties of Porous Media. In Hydrol. Pap., volume 3, Colorado State University, Fort Collins, 1964.

/CIN 06/ Cinar, Y., Pusch, G., Reitenbach, V.: Petrophysical and Capillary Properties of Compacted Salt, Transport in Porous Media (2006) 64: 199-228, Springer, 2006.

/ENG 12/ Engelhardt, H.J., Stradinger, A., v. Borstel, L.E.Bestimmung der Oberflächenfeuchte von Steinsalzgrus aus dem Erkundungsbergwerk Gorleben. Memo im Arbeitspaket 9.1.2, 2012 (listed in /FIS 13/)

/FIS 13/ Klaus Fischer-Appelt, K., Baltes, B., Buhmann, D., Larue, J., Mönig, J.: Sythesebericht für die VSG - Bericht zum Arbeitspaket 13. FKZ UM10A03200 (BMU), Gesellschaft für Anlagen- und Reaktorsicherheit (GRS) mbH, GRS-290, Köln, 2013.

/GEN 80/ Van Genuchten, M.T.: A Closed-Form Equation for predicting the hydraulic Conductivity of Unsaturated Soils. - Soil Sci. Soc. Am. J., 44:892-898, 1980.

/HAR 01/ Harrison, B., Jing, X.D.: Saturation Height Methods and Their Impact on Volumetric Hydrocarboni n Place. Proceedings - SPE Annual Technical Conference and Exhibition, 2001, Society of Petroleum Engineers (SPE), 2001.

/HEL 97/ Helmig, R.: Multiphase Flow and Transport Processes in the Subsurface. Springer, Berlin, 1997.

/KRÖ 09/ Kröhn, K.-P., Stührenberg, D., Herklotz, M., Heemann, U., Lerch, C., Xie, M.: Restporosität und -permeabilität von kompaktierendem Salzgrus-Versatz; Projekt REPOPERM - Phase 1. Abschlussbericht, FKZ 02 E 10477 (BMWi), Gesellschaft für Anlagen- und Reaktorsicherheit (GRS) mbH, GRS-254, Köln, 2009.

/KRÖ 15/ Kröhn, K.-P., Zhang, C.-L., Czaikowski, O., Stührenberg, D., Heemann, U.: The compaction behavior of salt backfill as a THM-process. FKZ 02 E 10740 (BMWi), in Roberts, L., Mellegard, K., Hansen, F. (eds.): Mechanical Behaviour of Salt VIII – Proceedings of the 8th Conference on the Mechanical Behaviour of Salt, SaltMechVIII, Rapid City, USA, CRC Press/Balkema, 2015.

/LEN 89/ Lenhard, R.J., Parker, J.C., Mishra, S.: On the Correspondence between Brooks-Corey and Van Genuchten Models. J. of Irrigation and Drainage Engineering, Heft 4, 1989.

/LEV 41/ Leverett, M. C.; Capillary behavior in porous solids; Petroleum Transactions of AIME (1941); 142; 152-169, 1941.

/MAL 15/ Malama, B.: Experimental Investigation of Two-Phase Flow in Consolidating and Intact Salt: Analysis of Capillary Pressure Measurements from Core Labs. Technical report SAND2015- 8116R, Sandia National Laboratories, Albuquerque, 2015.

/ROT 99/ Rothfuchs, T.; Feddersen, H.-K.; Kröhn, K.-P.; Miehe, R.; Wieczorek, K.: The DEBORA-Project: Development of Borehole Seals for High-Level Radioactive Waste - Phase II. Final report, FZK 02 E 8715, Gesellschaft für Anlagen- und Reaktorsicherheit (GRS) mbH, Bericht GRS-161, GRS Köln, 1999.

Appendix: Sample properties

All in all 10 samples had been prepared based on the crushed salt of d < 8 mm (see Appendix G). They were characterised with respect to bulk density and porosity. The results are compiled in Tab. F.5.

Additionally, the results concerning gas permeability and brine permeability are added in the table. Gas permeability was determined at different pressure gradients before the test to find comparable sets of samples. For further use the mean of all resulting values was calculated. During the test also the brine permeability was measured. For reference, these values are added to Tab. F.5 where applicable.

Tab. F.5 Characteristic sample properties

Sample identification internal / external		Length [cm]	Volume[‡] [cm³]	Mass [g]	Density [g/cm³]	Porosity [%]	Pore volume [cm³]	Gas permeability [m²]	Brine permeability [m²]
M1[†]					1.970				
M2	M1a	100.37/ 98.9[#]	194.501[#]	397.56/ 379.16[#]	1.955/ 1.949[#]	10.70[#]	20.81[#]	$1.369 \cdot 10^{-13}$/ $9.955 \cdot 10^{-14}$ [#]	
M3	P	100.0	196.35	397.20	2.023	7.33	14.40	$7.454 \cdot 10^{-15}$	$7.969 \cdot 10^{-15}$/ $4.9 \cdot 10^{-16}$ *
M4		100.3	196.94	396.97	2.011	7.66	15.09	$2.720 \cdot 10^{-14}$	$4.8427 \cdot 10^{-16}$
M5		100.3	196.94	396.95	2.016	7.67	15.10	$3.097 \cdot 10^{-14}$	$1.0011 \cdot 10^{-15}$
M6		100.6	197.53	396.07	2.005	8.15	16.09	$2.280 \cdot 10^{-14}$	
M7		100.1	196.55	396.07	2.015	7.69	15.11	$1.769 \cdot 10^{-14}$	
M8-B	M1b	100.0	196.35/ 189.42[#]	396.90	2.021/ 2.015[#]	7.40/ 7.69[#]	14.54/ 14.57[#]	$1.216 \cdot 10^{-14}$ [#]	
REP 3	M2a	100.35	193.10	395.94	2.050	6.1	11.731	$2.0 \cdot 10^{-15}$	$1.4 \cdot 10^{-15}$
REP 4	M2b	99.5	189.58	392.20	2.069	5.2	09.916	$1.1 \cdot 10^{-15}$	$2.5 \cdot 10^{-17}$

[†] only used for compaction optimisation
[‡] circular diameter was about 50 mm in all cases
[#] after installation and lathing
* post-test value